[9] F. Viani, L. Lizzi, R. Azaro, and A. Massa, "A miniaturized UWB antenna for wireless dongle devices," *IEEE Antennas Propag. Lett.*, vol. 7, pp. 714–717, 2008.
[10] L. Lizzi, F. Viani, R. Azaro, and A. Massa, "Optimization of a spline-shaped UWB antenna by PSO," *IEEE Antennas Propag. Lett.*, vol. 6, pp. 182–185, 2007.
[11] M. Benedetti, L. Lizzi, F. Viani, R. Azaro, P. Rocca, and A. Massa, "A linear antenna array for UWB applications," in *Proc. Antenna and Propag. Soc. Int. Symp.*, 2008, pp. 1–4.
[12] H. Sheng, P. Orlik, A. M. Haimovich, L. J. Cimini, and J. Zhang, "On the spectral and power requirements for ultra-wideband transmission," in *Proc. IEEE Int. Conf. Commun.*, 2003, pp. 738–742.
[13] J. Liang, L. Guo, C. C. Chiau, X. Chen, and C. G. Parini, "Study of a printed circular disk monopole antenna for UWB systems," *IEEE Trans. Antennas Propag.*, vol. 53, pp. 3500–3504, Nov. 2005.
[14] J. Liang, L. Guo, C. C. Chiau, X. Chen, and C. G. Parini, "Study of CPW-fed disk monopole antenna for ultra wideband applications," in *IEE Proc. Microwave Antenna Propag.*, Dec. 2005, vol. 152, pp. 520–526.
[15] A. Mehdipour, K. Mohammadpour-Aghdam, and R. Faraji-Dana, "Complete dispersion analysis of Vivaldi antenna for ultra wideband applications," *Progr. Electromagn. Res.* pp. 85–96, 2007 [Online]. Available: http://ceta.mit.edu/PIER
[16] X. King, Z. N. Chen, and M. Y. W. Chia, "Parametric study of ultra-wideband dull elliptically tapered antipodal slot antenna," *Int. J. Antenna Propag.*, vol. 2008, Article ID: 267197.
[17] M. Kanda, "Time domain sensors and radiators," in *Time Domain Measurement in Electromagnetics*, E. K. Miller, Ed. New York: Van Nostrand Reinhold, 1986, ch. 5.

Optimized Microstrip Antenna Arrays for Emerging Millimeter-Wave Wireless Applications

Behzad Biglarbegian, Mohammad Fakharzadeh, Dan Busuioc, Mohammad-Reza Nezhad-Ahmadi, and Safieddin Safavi-Naeini

***Abstract*—Two compact planar antennas operating in the unlicensed 60 GHz frequency band are presented based on the physical layer specifications of IEEE 802.15.3c and ECMA 387 standards for different classes of wireless applications. Each antenna is an array of 2×2 microstrip antennas covering at least two channels of the 60 GHz spectrum. The first antenna is optimized to achieve the highest gain, while the second antenna is optimized to give the largest beamwidth. The maximum measured radiation gain of the first antenna is 13.2 dBi. The measured beamwidth and gain of the second antenna are 76° and 10.3 dBi, respectively. The areas of these two antenna are only 0.25 and 0.16 cm^2. The variation of radiation gain of each antenna over the frequency range of 57–65 GHz is less than 1 dB.**

***Index Terms*—IEEE 802.15.3c, microstrip patch antenna, wireless communication, 60 GHz.**

I. Introduction

Recently antenna design for 60 GHz short-range wireless communication has become a subject of great interest [1]–[11]. Many of these antennas do not satisfy some of the requirements enforced by the recent 60 GHz standards such as IEEE 802.15.3c [12] released in December 2009, and ECMA 387 [13]. Therefore, antenna design for 60 GHz applications will remain a hot research area for next few years.

For emerging mass market millimeter-wave radio networks, system-on-chip radio modules integrated with compact planar antenna seem to be an attractive solution. A number of on-chip or in-package 60 GHz antennas have been reported so far [2], [3]. They are generally low-gain/low-radiation efficiency structures. Given very low transmitted power and poor receiver sensitivity of low-cost millimeter-wave technologies, such antennas can not mitigate the severe path loss, which is close to 88 dB for 10 m range at 60 GHz. Some of the designed antennas have a narrow beam [4] (30°), which makes them suitable only for point-to-point applications.

Compatibility with the emerging standards for the 60 GHz spectrum is the starting point for the antenna design. Narrowband or low-gain antennas do not comply with the aforementioned standard requirements. For example, the bandwidth of an active antenna for WPAN applications in [1] is about 0.8 GHz which is below the bandwidth requirement for 60 GHz devices (around 2 GHz). Finally, fabrication cost and complexity of the antenna is another major issue which affects its usability. In [8] a high gain and an acceptable bandwidth have been achieved by a CPW-fed integrated horn antenna with a simulated gain of 14.6 dBi. However the size of this end-fire antenna is 32 mm × 20 mm and requires a complex fabrication process.

For the first time, based on the analysis of the two proposed standards for 60 GHz wireless systems, IEEE 802.15.3c and ECMA 387, this work attempts to develop low-cost optimal antenna structures, which can deliver the required antenna gain, bandwidth and the beamwidth. Thus, two optimized, 2×2 compact microstrip array antennas are presented. The first antenna is optimized for point-to-point applications which require a high gain antenna. A maximum gain of 13.2 dBi has been measured for an area of 0.25 cm^2. The second antenna is optimized for point-to-multipoint applications requiring a wide beam. The measured beamwidth of this antenna exceeds 76° for an area of only 0.16 cm^2. Both antennas cover at least two channels of the 60 GHz spectrum. The developed antennas can be considered as low-cost and low-profile (planar) solution for various classes of services described in IEEE 802.15.3c and ECMA 387 standards.

The organization of this communication is as follows. Section II briefly reviews the IEEE and ECMA standards to extract the required parameters for 60 GHz antenna design. Section III describes the design and optimization of high-gain and fan-beam patch arrays. Section IV presents the measured results, and Section V concludes this communication.

II. Required Antenna Characteristics for IEEE and ECMA Standards

For 60 GHz short-range wireless communications two standard drafts, IEEE 802.15.3c and ECMA 387, have been released so far. IEEE 802.15.3c defines three classes for different wireless (single carrier) applications [12]:

- Class 1 addresses the low-power low-cost mobile market with a relatively high data rate of up to 1.5 Gb/s;
- Class 2 supports for data rates up to 3 Gb/s;
- Class 3 supports high performance applications with data rates in excess of 5 Gb/s.

Similar to IEEE 802.15.3c, ECMA 387 defines three types of devices (Type A, B and C) for 60 GHz spectrum [13] based on the operational requirements such as maximum range, bit rate and system complexity. Several operational modes have been proposed for each type. Table I shows the requirements of the basic and highest-rate modes of each

Manuscript received March 16, 2010; revised September 14, 2010; accepted October 26, 2010. Date of publication March 03, 2011; date of current version May 04, 2011. This work was supported by the National Science and Engineering Research Council of Canada (NSERC) and Research in Motion (RIM).

The authors are with the Department of Electrical and Computer Engineering, University of Waterloo, Waterloo, ON N2L3G1 Canada (e-mail: bbiglarb@maxwell.uwaterloo.ca).

Color versions of one or more of the figures in this communication are available online at http://ieeexplore.ieee.org.

Digital Object Identifier 10.1109/TAP.2011.2123058

TABLE I
MODE DEPENDENT PARAMETERS OF TYPE A, B, AND C DEVICES IN ECMA STANDARD

Mode	Max. Range	RX Sensitivity	Data-Rate	Constellation
A0	10 m	-60 dBm	0.397 Gb/s	BPSK
A9	$<$ 10 m	-40.7 dBm	6.35 Gb/s	16-QAM
B0	3 m	-60.7 dBm	0.794 Gb/s	DBPSK
B2	$<$ 3 m	-54.6 dBm	3.175 Gb/s	DQPSK
C0	1 m	-62.2 dBm	0.8 Gb/s	OOK
C2	$<$ 1 m	-53.5 dBm	3.2 Gb/s	4ASK

TABLE II
mm-WAVE PHYSICAL CHANNELIZATION

Channel	1	2	3	4
Frequency	57.24-59.4	59.4-61.56	61.56-63.72	63.72-65.88

device type. In the following, the main parameters of the physical layer of these two standards, which must be considered in the antenna design, are discussed.

A. Antenna Bandwidth

In both standards, the 60 GHz spectrum has been divided into four channels, shown in Table II. Each channel has a bandwidth of 2.16 GHz. Any device must support at least one channel. In North America, the first three channels have been released. Channel four has been released in Japan and Europe.

B. Antenna Gain

In a communication link, if the same antennas are used for both transmitter and receiver ($G_R = G_T = G_a$), then the transmitter power (P_T) is related to the antenna gain, receiver sensitivity ($S_{\min}$) and path loss (PL) by

$$P_T + 2G_a \geq S_{\min} - PL \tag{1}$$

where P_T and $S_{\min}$ are in dBm and G_a and PL are in dB. The right-hand side (RHS) of (1) is determined by the standard. But the left-hand side (LHS) gives a freedom to the designer to choose the suitable power amplifier and antenna.

Fig. 1 demonstrates the transmitter power versus the antenna gain at 60 GHz for the basic modes described in Table I, for LOS links. This figure also shows the FCC limit on the indoor EIRP (document 47 CFR 15.255).

For an integrated RFIC the transmitted power is limited by the semiconductor processing technology. The horizontal lines in Fig. 1 show the typical technology limits for CMOS technology (0–10 dBm). Fig. 1 shows that for CMOS-compatible Type C devices a low gain antenna ($G_a \leq 2.7$ dBi) is sufficient. For Type B devices in CMOS the antenna gain can vary from 3.3 to 8.3 dBi. However for Type A, which is considered as the *high end-high performance* device [13], a high-gain antenna is necessary. An antenna with an affective gain of 13.7 dBi at 57 GHz for $P_T = 0$ dBm is ideal for mode A0 operating at the maximum range of 10 m. For transmitting higher bit-rates at the maximum range either an array of such antenna can be used or the transmitter power can be increased. Therefore, one of the objectives of this communication is to design a compact antenna with a maximum gain above 13 dBi. The RX-TX antenna polarization mismatch or misalignment can be compensated by a small increase (1–3 dB) in the transmitter power.

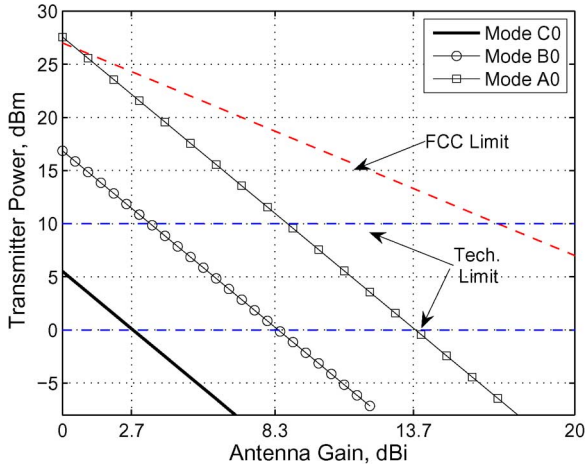

Fig. 1. Transmitter power versus antenna gain for different operational modes at 57 GHz.

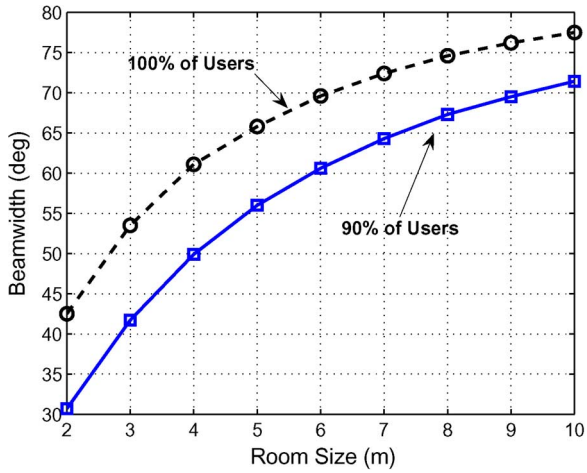

Fig. 2. Finding the beamwidth of the antenna. (a) Simulated scenario. (b) Antenna angular coverage versus room size for uniform user distribution.

C. Antenna Beamwidth

For 60 GHz applications antennas with higher gains (e.g., 13.7 dBi for Type A) are required, which have directional patterns. For certain receivers connecting to an Access Point (AP) in a room, such as cell phone or laptop, an omni pattern is not required.

Assume a square room with a size of $l \times l$ and the height of 3.5 m. An AP has been installed at the center of ceiling with a hemispherical pattern. It is also assumed that the user distribution along the z-coordinate is uniform ranging within 1.5 to 2.5 m from ceiling (AP). To find the required coverage angle, 20 000 random user locations were generated. The angle between the line connecting the user to AP and z axis was calculated for each user, and the histogram of all calculated angles was plotted. Fig. 2 shows the required values for beamwidth to cover 90% and 100% of the indoor users versus room size ($2 \leq l \leq 10$) for uniform user distribution. For the maximum room size (10 m), the RX antenna coverage must be respectively 72° and 77.5° to include 90% and 100% of users.

III. ANTENNA DESIGN AND OPTIMIZATION

Although employing a high-gain antenna relaxes the signal to noise requirement of the front-end RF system, its narrow beam can not cover

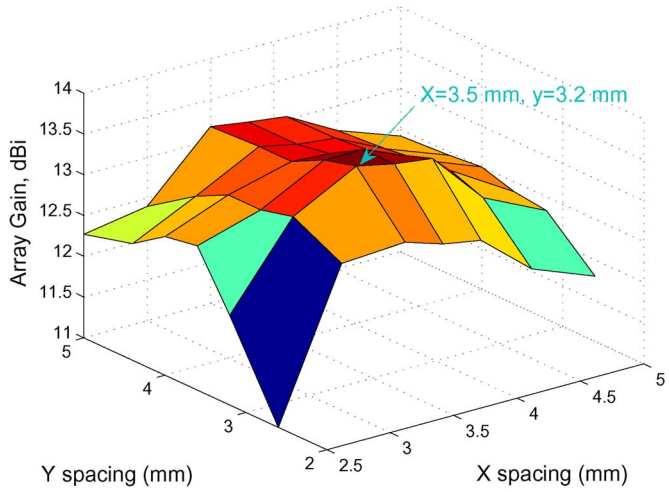

Fig. 3. Antenna array gain versus patch spacing.

the entire zone for point-to-multipoint wireless connections. In this section two antennas for different 60 GHz applications are proposed based on the IEEE 802.15.3c and ECMA 387 standards. The first antenna is designed for the maximum gain for point-to-point applications over the maximum distance of 10 m. The second antenna is optimized to give the maximum beamwidth for point-to-multipoint applications such as WPAN. Each antenna is an array of four patch elements. The distances between patch elements are optimized to obtain the maximum gain or beamwidth.

Patch antenna is a planar, high-gain and efficient radiator that can be integrated easily with the rest of the system. A single rectangular patch antenna typically provides 7 dB gain and more than 100° beamwidth when its fundamental mode (TM10) is excited [14].

In this communication, a very low loss substrate (RT/duroid-5880) with 10 mil height, $\tan\delta = 1 \times 10^{-3}$ and dielectric constant of $\epsilon_r = 2.2$ is used as the substrate for microstrip antennas and the feeding lines. The patch and the ground plane are printed on the top and bottom of the dielectric substrate, respectively. The dimensions of the single patch antenna on such substrate is optimized to achieve the maximum gain at 60 GHz. The size of the patch element is 1.85×1.45 mm^2. The simulations in Ansoft HFSS show that this single patch has 7.7 dBi gain at 60 GHz. The simulated HPBW in E-plane exceeds 96°, but the HPBW in H-plane is limited to 68°.

A. High-Gain Antenna Design

In this section an array of four patch antennas is formed and the x and y spacings between antennas are optimized to achieve the highest gain. Fig. 3(a) shows the 2×2 patch array gain versus patch spacing at 60 GHz obtained by HFSS simulation. It is seen that the maximum gain of 13.5 dBi is achieved for $x = 3.5$ mm and $y = 3.2$ mm. The effect of feed network on the array gain is also studied. After optimization, it is seen that the maximum gain is obtained for $a_1 = 0.2$ mm and $b_1 = 0.45$ mm. Parameters a_1 and b_1 are shown in Fig. 4(a). As shown in Fig. 4(a) the size of the patch array for the optimized spacings is 5.35 mm × 4.65 mm. Fig. 4(b) shows the reflection coefficient of this array. It is seen that this antenna covers two channels of the 60 GHz spectrum from 57.24 to 61.46 GHz. The return loss is always more than 7.5 dB. The resonance frequency is at 59.4 GHz, the common edge of the two adjacent channels, therefore the most efficient use of the antenna bandwidth has been achieved. Fig. 5(a) and (b) shows the 2D and 3D radiation patterns of the high-gain 2×2 patch array. The 3 dB beamwidth of the array in $\phi = 0°$ plane ($x-z$ plane) and $\phi = 90°$ ($y-z$ plane) are 41° and 36°, respectively. The first pair of nulls happen

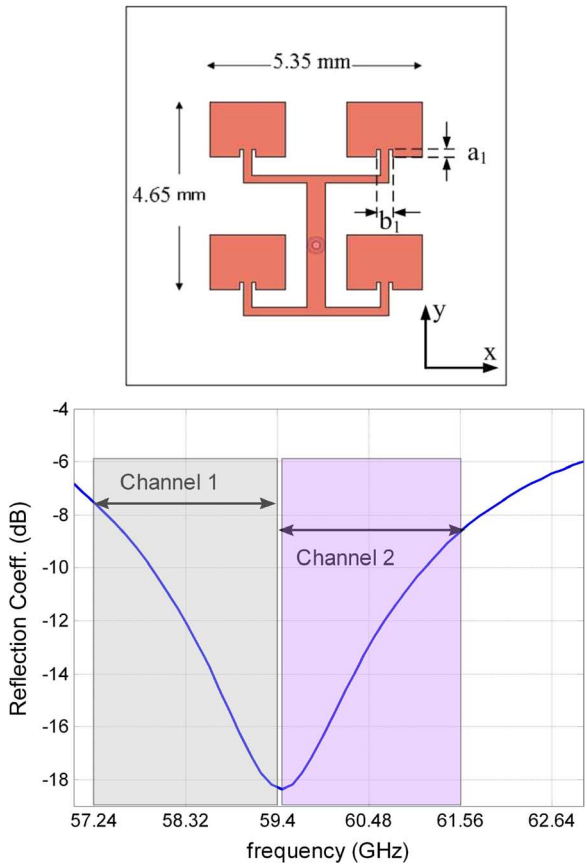

Fig. 4. (a) Top view of the high-gain 2×2 patch array. (b) Reflection coefficient of this antenna.

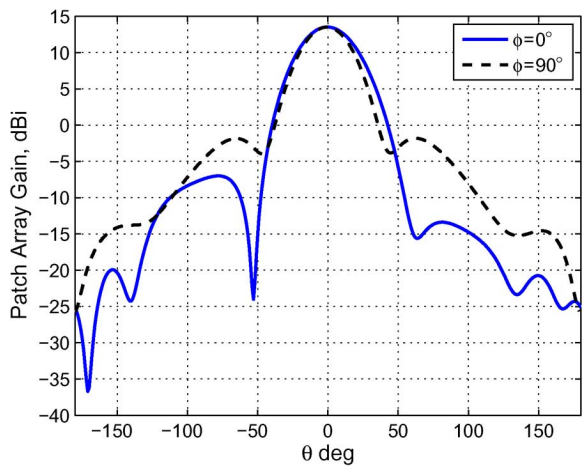

Fig. 5. 2D radiation pattern of the high-gain 2×2 patch array.

approximately at $\pm 50°$. Fig. 5(b) shows that the radiation pattern is symmetric around the normal axis.

B. Fan-Beam Antenna Design

To achieve the required beamwidth of 77.5°, discussed in Section II-C, another patch array is designed and the element spacing is optimized to obtain the maximum beamwidth.

Table III shows the maximum gain of 2×2 array at 57 GHz for different element spacings. It is seen that the gain increases with the element spacing since the effective aperture size increases. For

TABLE III
MAXIMUM GAIN OF FAN-BEAM PATCH ARRAY VERSUS ELEMENT-SPACING

X (mm)	2	2.2	2.4	2.6	2.8	3
Y=2.2 mm	9.35	9.57	9.81	10.05	10.3	10.53
Y=2.3 mm	9.5	9.65	9.9	**10.17**	10.43	10.55
Y=2.4 mm	9.52	9.67	9.91	10.28	10.44	10.62
Y=2.5 mm	9.63	9.7	9.94	10.18	10.25	10.55

TABLE IV
BEAMWIDTH OF FAN-BEAM PATCH ARRAY IN E-PLANE

X (mm)	2	2.2	2.4	2.6	2.8	3
Y=2.2 mm	83°	81°	80°	80°	79°	79°
Y=2.3 mm	80°	79°	78°	**78°**	76°	75°
Y=2.4 mm	77°	78°	76°	75°	75°	73°
Y=2.5 mm	75°	75°	75°	74°	74°	74°

TABLE V
BEAMWIDTH OF FAN-BEAM PATCH ARRAY IN H-PLANE

X (mm)	2	2.2	2.4	2.6	2.8	3
Y=2.2 mm	55°	50°	49°	46°	44°	40°
Y=2.3 mm	53°	50°	49°	**46°**	43°	41°
Y=2.4 mm	54°	51°	49°	46°	43°	40°
Y=2.5 mm	55°	51°	49°	46°	43°	41°

$y \geq 2.6$ mm the maximum gain is always above 10 dBi. We choose $G_a \geq 10$ dBi as a criterion to find the optimum patch spacing. If a higher gain was required two of these fan-beam antennas can be arrayed in the y-direction to give around 13 dBi gain while the maximum beamwidth at $\phi = 0°$ surface is unaffected. Table III indicates that the element spacing along x axis must be equal or larger than 2.6 mm to obtain 10 dBi gain. Table IV and Table V present the patch array beamwidth in E-plane and H-plane versus element spacing. The beamwidth in E-plane reduces as the element spacing increases; however, the beamwidth in H-plane is almost insensitive to x-spacing for the values shown in Table V. We choose the spacings which lead to the largest E-plane beamwidth while the gain is above 10 dBi. Table IV shows that for $x = 2.6$ mm and $y = 2.3$ mm a beamwidth of 78° is achieved. The size of the patch array, shown in Fig. 6(a), for the optimized spacings is 4.45 mm × 3.7 mm. Fig. 6(b) shows the reflection coefficient of the fan-beam 2 × 2 patch array. The resonant frequency of the antenna is at 59.5 GHz, and the 10 dB bandwidth covers channel 1 and 2 of the 60 GHz spectrum. Fig. 7 shows the 2D and 3D radiation patterns of the fan-beam 2 × 2 patch array. The 3 dB beamwidths of the array in E-plane and H-plane are 78° and 46°, respectively. The first pair of nulls are far away from the maximum gain direction at ±90°. Hence, any possible rotation or misalignment of the antenna cannot nullify the received signal. Fig. 7(b) shows that the radiation pattern in $y - z$ plane is symmetric, while the pattern in $x - z$ plane is asymmetric due to the feed line effect.

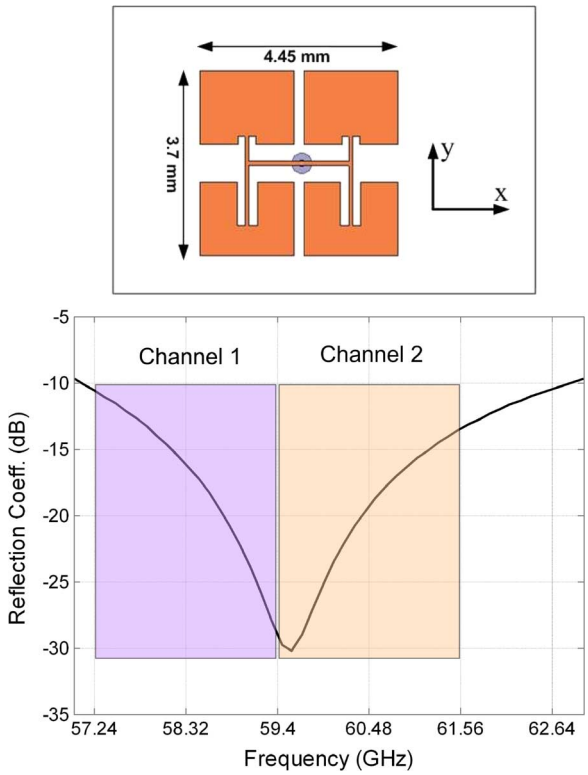

Fig. 6. (a) Top view of the fan-beam 2 × 2 patch array. (b) Reflection coefficient of this antenna.

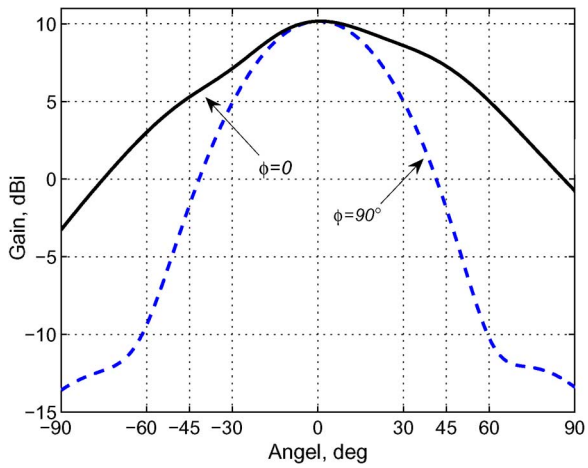

Fig. 7. 2D radiation pattern of the fan-beam 2 × 2 patch array.

IV. FABRICATION AND MEASUREMENTS

This section describes the test set-up and presents the measured results of both patch antenna arrays.

A. High-Frequency Waveguide to Microstrip Transition

Accurate measurement requires minimal interconnect loss between various parts of the test setup. Most of the measuring systems at mm-wave frequency have WR-15 waveguide ports, therefore in this work a low insertion/reflection loss waveguide to microstrip transition (WMT) at 60 GHz band is developed for characterization of the patch antenna arrays.

To lower the fabrication cost, a two-part machined metallic structure made out of Aluminum was designed and fabricated for the transition. For the microstrip antenna connection, a perpendicular coaxial transition was developed. This configuration was preferred to an end-launch type due to the easier implementation and better narrowband matching. The cost is also reduced by using simple Corning glass-based 50-ohm coax probes that connect the waveguide section to the microstrip antenna. The narrow air-gap between the two parts of the waveguide assembly creates a discontinuity in the surface current of dominant TE10 mode. This could potentially increase the loss. As a remedy a larger number of sealing screws and a raised ridge was used. The drawing

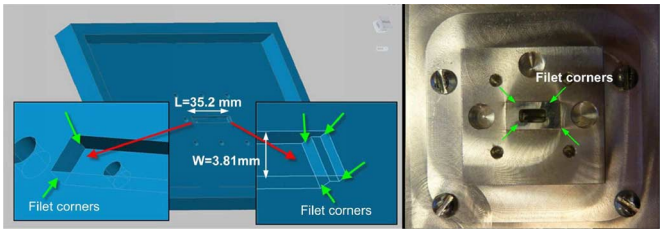

Fig. 8. Transition design features and manufacturing implementation.

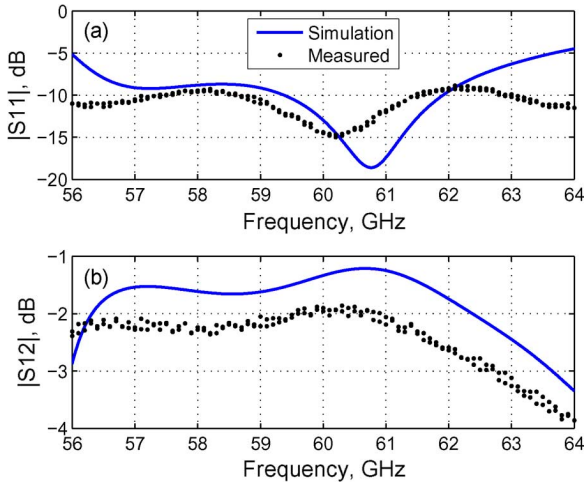

Fig. 9. Performance of the back-to-back configuration of two microstrip to waveguide transitions. (a) S_{11}. (b) Insertion loss S_{21}.

and the picture of the developed WMT are illustrated in Fig. 8. The channel length of WR-15 waveguide section is chosen for mechanical convenience. Note that the channel length (L) must include a $0.25\lambda_g$ (the quarter guided wavelength in the waveguide) section between the probe location and the shorted section of the waveguide optimized for matching. In our case, the total waveguide length is close to 7λ (or 35.2 mm). To determine the performance of this WMT, two identical structures are connected in a back-to-back configuration and tested. The measurement setup involves two WR-15 type waveguides, which are calibrated in a 2-port setup, and a coaxial two-sided probe to mate these two identical structures. Fig. 9(a) and (b) compares the simulated and measured S_{11} and S_{21} of the back-to-back configuration. The measured transmission S_{21} illustrates that at 60 GHz the insertion loss of this configuration is close to 2.0 dB, which indicates that a single WMT has around 1.0 dB loss. The information provided by Fig. 9(b) is used to de-embed the insertion loss of WMT from the measured antenna gain in next section.

B. Measurement Results

Fig. 10 shows the fabricated 2 × 2 patch antenna arrays. The antennas were mounted and attached to the transitions described earlier. The antennas combined with WMT were simulated in HFSS to see the effects of the transition on the reflection coefficient of the antennas. Fig. 11(a) and (b) shows the measured and simulated S_{11} of the high-gain and fan-beam 2 × 2 patch antenna arrays, respectively. The bandwidth of the high-gain and fan-beam antennas are 3.5 and 3.6 GHz around 60 and 61.70 GHz, respectively. As it is shown in both figures, there are more than one resonances over the frequency range 50–75 GHz. These resonances show the nonradiating cavity modes of

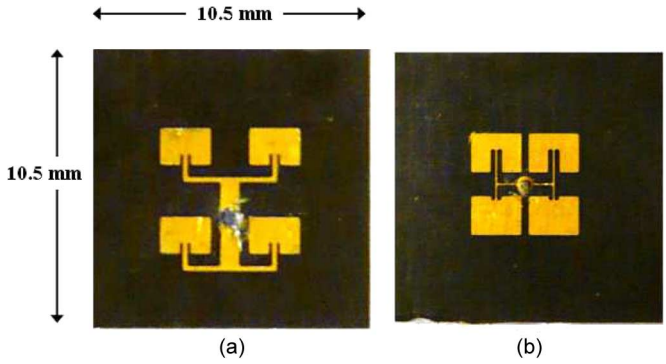

Fig. 10. Fabricated high-gain and fan-beam 2 × 2 patch array antennas.

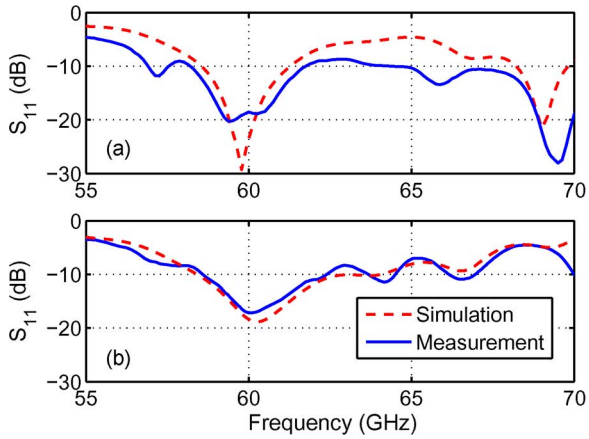

Fig. 11. S_{11} Simulation and measurement results of the 2 × 2 patch array antennas connected to the waveguide transitions. (a) High-gain antenna. (b) Fan-beam antenna.

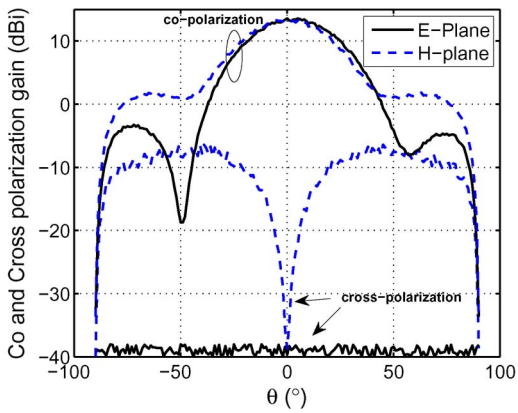

Fig. 12. Measured co-polarization and cross-polarization radiation patterns of the high-gain 2 × 2 patch antenna arrays at 60 GHz frequency.

the waveguide section of WMT. This was experimentally verified by using absorbers to suppress the radiating fields into free space. While the resonances of the radiating modes were affected significantly, the non-radiating cavity modes did not change, enormously. Comparing these figures to Fig. 4(b) and Fig. 6(b) and considering the good agreement of HFSS simulations and the measurement results, we can conclude that the array antennas without WMT meet the required bandwidth specifications for the aforementioned wireless standards.

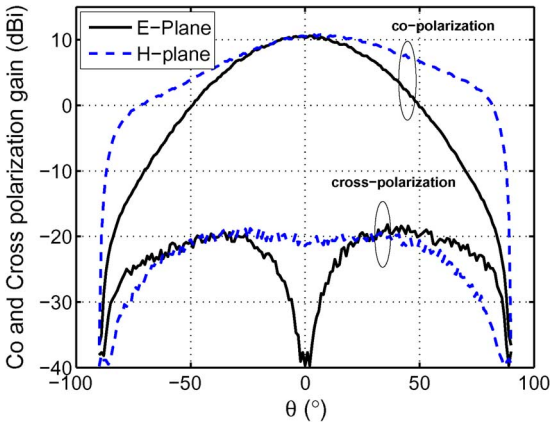

Fig. 13. Measured co-polarization and cross-polarization radiation patterns of the fan-beam 2 × 2 patch array at 60 GHz frequency.

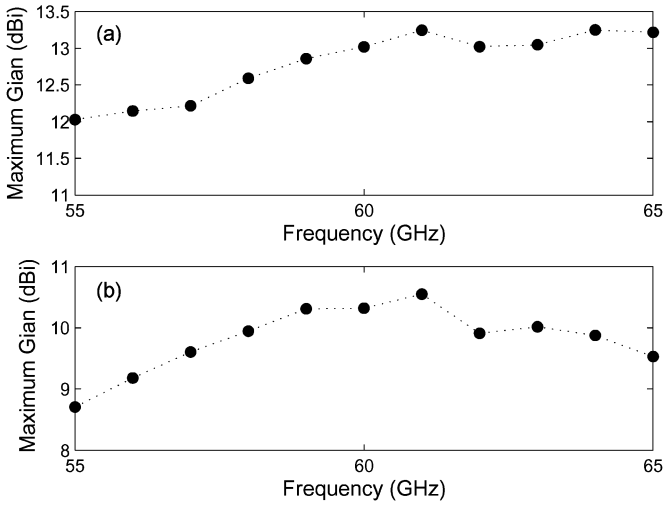

Fig. 14. Measured maximum gain of patch antenna arrays over the frequency range of 55–65 GHz. (a) High-gain array. (b) Fan-beam array.

Fig. 12 shows the measured co-polarization and cross-polarization radiation pattern of the high-gain 2 × 2 patch antenna array at 60 GHz frequency. The maximum measured gain at this frequency is 13 dBi after de-embedding the insertion loss of WMT (see Fig. 9) and considering 0.3 dB loss for the coaxial probe which feeds the antenna. The measured beamwidth is 42°. Comparing this figure to Fig. 5(a) which shows the simulated gain and radiation pattern, it is found that the maximum gain at 60 GHz has dropped by only 0.5 dB. The measured beamwidth and overall pattern shape are in very good agreement with the simulated values. The maximum cross-polarization gain of the high-gain array with respect to its co-polarization gain is at least −10 dB which is at $\theta = 40°$. Fig. 13 depicts the measured co-polarization and cross-polarization radiation pattern of the fan-beam antenna at 60 GHz. The HPBW of the fan-beam antenna is 76° and its maximum gain is 10.3 dBi. Comparing this figure to Fig. 7 shows that the agreement between simulated and measured patterns is very good. The beamwidth has slightly decreased (by about 2 degrees) which is within the fabrication tolerances. The cross polarization gain of the fan-beam array antenna is at least 25 dB less than co-polarization term at any direction. Fig. 14 depicts the measured maximum gain of patch antenna arrays over the frequency range of 55–65 GHz after de-embedding the insertion loss of WMT. The maximum gain of the high-gain array varies from 12.25 dBi at 57 GHz to 13.25 dBi at 65 GHz. For the fan-beam array, the maximum gain varies from 9.5 dBi at 57 GHz to to 10.5 dBi at 61 GHz. So, the variation of the radiation gain of both antennas over 7 GHz bandwidth (57–64 GHz) is less than 1 dB.

V. Conclusion

In this communication, the two optimized 2 × 2 patch array antennas for emerging millimeter-wave radio networks were presented. Based on IEEE 802.15.3c and ECMA 387 standards, the radiation characteristics of the antenna such as gain, bandwidth and beamwidth have been derived. The developed antennas fully meet the requirements for the point-to-point line-of-sight applications and maximum signal coverage. The measured results of the high-gain antenna show more than 13 dBi gain, and 3.5 GHz of impedance bandwidth including the microstrip to waveguide transition. Furthermore, the developed fan-beam antenna has more than 10 dBi gain with 76° beamwidth in E-plane and 3.6 GHz impedance bandwidth. The variation of the maximum radiation gain of both antennas over the whole 7 GHz spectrum is less than 1 dB. These two antennas can be easily integrated with phase shifters to form high-gain array antennas with beam-scanning capabilities.

Acknowledgment

The authors would like to acknowledge Dr. G. Rafi for his invaluable support regarding the antenna measurements.

References

[1] C. Karnfelt, P. Hallbjorner, H. Zirath, and A. Alping, "High gain active microstrip antenna for 60-GHz WLAN/WPAN applications," *IEEE Trans. Microw. Theory Tech.*, vol. 54, no. 6, pp. 2593–2603, Jun. 2006.

[2] I.-S. Chen, H.-K. Chiou, and N.-W. Chen, "V-band on-chip dipole-based antenna," *IEEE Trans. Antennas Propag.* , vol. 57, no. 10, pp. 2853–2861, Oct. 2009.

[3] Y. Zhang, M. Sun, and L. Guo, "On-chip antennas for 60-GHz radios in silicon technology," *IEEE Trans. Electron Devices*, vol. 52, no. 7, pp. 1664–1668, Jul. 2005.

[4] Y. P. Zhang, M. Sun, K. M. Chua, L. L. Wai, and D. Liu, "Antenna-in-package design for wirebond interconnection to highly integrated 60-GHz radios," *IEEE Trans. Antennas Propag.*, vol. 57, no. 10, pp. 2842–2852, Oct. 2009.

[5] K.-C. Huang and D. Edwards, "60 GHz multibeam antenna array for gigabit wireless communication networks," *IEEE Trans. Antennas Propag.*, vol. 54, no. 12, pp. 3912–3914, Dec. 2006.

[6] A. Rosen, R. Amantea, P. Stabile, A. Fathy, D. Gilbert, D. Bechtle, W. Janton, F. McGinty, J. Butler, and G. Evans, "Investigation of active antenna arrays at 60 GHz," *IEEE Trans. Microw. Theory Tech.*, vol. 43, no. 9, pp. 2117–2125, Sep. 1995.

[7] A. Lamminen, J. Saily, and A. Vimpari, "60-GHz patch antennas and arrays on LTCC with embedded-cavity substrates," *IEEE Trans. Antennas Propag.*, vol. 56, no. 9, pp. 2865–2874, Sep. 2008.

[8] B. Pan, Y. Li, G. Ponchak, J. Papapolymerou, and M. Tentzeris, "A 60-GHz CPW-fed high-gain and broadband integrated horn antenna," *IEEE Trans. Antennas Propag.*, vol. 57, no. 4, pp. 1050–1056, Apr.l 2009.

[9] A. Patrovsky and K. Wu, "Active 60 GHz front-end with integrated dielectric antenna," *Electron. Lett.*, vol. 45, no. 15, pp. 765–766, 2009, 16.

[10] Y. Murakami, T. Kijima, H. Iwasaki, T. Ihara, T. Manabe, and K. Iigusa, "A switchable multi-sector antenna for indoor wireless LAN systems in the 60-GHz band," *IEEE Trans. Microw. Theory Tech.*, vol. 46, no. 6, pp. 841–843, Jun. 1998.

[11] P. Smulders and M. Herben, "A shaped reflector antenna for 60-GHz radio access points," *IEEE Trans. Antennas Propag.*, vol. 49, no. 7, pp. 1013–1015, Jul. 2001.

[12] IEEE, IEEE 802.15 WPAN Task Group 3c (TG3c) Sept. 2009 [Online]. Available: http://www.ieee802.org/15/pub/TG3c.html

[13] ECMA, Standard ECMA-387: High Rate 60 GHz PHY, MAC and HDMI PAL Dec. 20081st ed. [Online]. Available: http://www.ecma-international.org/publications/files/ECMA-ST/Ecma-387.p df

[14] J. R. James and P. S. Hall, *Handbook of Microstrip Antennas*. London, U.K.: Inst. Elect. Eng. (IEE), 1989.